Approaching single temporal mode operation in twin beams generated by pulse pumped high gain spontaneous four wave mixing

Nannan Liu,[1] Yuhong Liu,[1] Xueshi Guo,[1] Lei Yang,[1] Xiaoying Li,[1*] Z. Y. Ou[2]

[1]*College of Precision Instrument and Opto-electronics Engineering, Tianjin University, Key Laboratory of Optoelectronics Information Technology of Ministry of Education, Tianjin 300072, China*

[2]*Department of Physics, Indiana University-Purdue University Indianapolis, Indianapolis, IN 46202, USA*

[*]*xiaoyingli@tju.edu.cn*

Abstract: By investigating the intensity correlation function, we study the spectral/temporal mode properties of twin beams generated by the pulse-pumped high gain spontaneous four wave mixing (SFWM) in optical fiber from both the theoretical and experimental aspects. The results show that the temporal property depends not only on the phase matching condition and the filters applied in the signal and idler fields, but also on the gain of SFWM. When the gain of SFWM is low, the spectral/temporal mode properties of the twin beams are determined by the phase matching condition and optical filtering and are usually of multi-mode nature, which leads to a value larger than 1 but distinctly smaller than 2 for the normalized intensity correlation function of individual signal/idler beam. However, when the gain of SFWM is very high, we demonstrate the normalized intensity correlation function of individual signal/idler beam approaches to 2, which is a signature of single temporal mode. This is so even if the frequencies of signal and idler fields are highly correlated so that the twin beams have multiple modes in low gain regime. We find that the reason for this behavior is the dominance of the fundamental mode over other higher order modes at high gain. Our investigation is useful for constructing high quality multi-mode squeezed and entangled states by using pulse-pumped spontaneous parametric down-conversion and SFWM.

OCIS codes: (270.0270) Quantum optics; (190.4380) Nonlinear optics, four-wave mixing; (320.7140) Ultrafast processes in fibers.

References and links

1. R. E. Slusher, P. Grangier, and A. Laporta, "Pulsed squeezed light," Phys. Rev. Lett. **59**, 2566–2569 (1987).
2. M. Fiorentino, P. L. Voss, J. E. Sharping, and P. Kumar, "All-fiber photon-pair source for quantum communication," Photon. Technol. Lett. **14**, 983–985 (2002).
3. Y. Shih, "Entangled biphoton source-property and preparation," Rep. Prog. Phys. **66**, 1009–1044 (2003).
4. J. Wenger, R. Tualle-Brouri, and P. Grangier, "Pulsed homodyne measurement of femtosecond squeezed pulses generated by single-pass parametric deamplification," Opt. Lett. **29**, 1267–1269 (2004).

#253936 Received 16 Nov 2015; revised 20 Dec 2015; accepted 5 Jan 2016; published 13 Jan 2016

5. W. Wasilewski, A. I. Lvovsky, K. Banaszek, and C. Radzewicz, "Pulsed squeezed light: Simultaneous squeezing of multiple modes," Phys. Rev. A **73**, 063819 (2006).
6. A. Eckstein, A. Christ, P. J. Mosley, and C. Silberhorn, "Highly efficient single-pass source of pulsed single-mode twin beams of light," Phys. Rev. Lett. **106**, 013603 (2011).
7. X. Guo, X. Li, N. Liu, L. Yang, and Z. Y. Ou, "An all-fiber source of pulsed twin beams for quantum communication," Appl. Phys. Lett. **101**, 261111 (2012).
8. Z. Y. Ou, J. K. Rhee, and L. J. Wang, "Photon bunching and multiphoton interference in parametric down-conversion," Phys. Rev. A **60**, 593–604 (1999).
9. Z. Y. Ou, "Parametric down-conversion with coherent pulse pumping and quantum interference between independent fields," Quantum Semiclass Opt. **9**, 599–614 (1997).
10. W. P. Grice, A. B. U'Ren, and I. A. Walmsley, "Eliminating frequency and space-time correlations in multiphoton states," Phys. Rev. A **64**, 063815 (2001).
11. A. B. U'Ren, C. Silberhorn, K. Banaszek, I. A. Walmsley, R. Erdmann, W. P. Grice, and M. G. Raymer, "Generation of pure-state single-photon wavepackets by conditional preparation based on spontaneous parametric downconversion," Laser Phys. **15**, 146–161 (2005).
12. D. Bouwmeester, J. W. Pan, K. Mattle, M. Eibl, H. Weinfurter, and A. Zeilinger, "Experimental quantum teleportation," Nature **390**, 575–578 (1997).
13. J. W. Pan, D. Bouwmeester, H. Weinfurter, and A. Zeilinger, "Experimental entanglement swapping: entangling photons that never interacted," Phys. Rev. Lett. **80**, 3891–3894 (1998).
14. E. Knill, R. Laflamme, and G. J. Milburn, "A scheme for efficient quantum computation with linear optics," Nature **409**, 46–52 (2001).
15. O. Pinel, P. Jian, R. M. de Araújo, J. Feng, B. Chalopin, C. Fabre, and N. Treps, "Generation and characterization of multimode quantum frequency combs," Phys. Rev. Lett. **108**, 083601 (2012).
16. X. Guo, N. Liu, X. Li, and Z. Y. Ou, "Complete temporal mode analysis in pulse-pumped fiber-optical parametric amplifier for continuous variable entanglement generation," Opt. Express **23**, 29369–29384 (2015).
17. B. Lamine, C. Fabre, and N. Treps, "Quantum improvement of time transfer between remote clocks," Phys. Rev. Lett. **101**, 123601 (2008).
18. K. Y. Spasibko, T. S. Iskhakov, and M. V. Chekhova, "Spectral properties of high-gain parametric down-conversion," Opt. Express **20**, 7507–7515 (2012).
19. T. S. Iskhakov, K. Y. Spasibko, M. V. Chekhova, and G. Leuchs, "Macroscopic hong-ou-mandel interference," New J. Phys. **15**, 093036 (2013).
20. A. Allevi, O. Jedrkiewicz, E. Brambilla, A. Gatti, J. Peřina, O. Haderka, and M. Bondani, "Coherence properties of high-gain twin beams," Phys. Rev. A **90**, 063812 (2014).
21. P. Sharapova, A. M. Peŕez, O. V. Tikhonova, and M. V. Chekhova, "Schmidt modes in the angular spectrum of bright squeezed vacuum," Phys. Rev. A **91**, 043816 (2015).
22. I. V. Dyakonov, P. R. Sharapova, T. S. Iskhakov, and G. Leuchs, "Direct Schmidt number measurement of high-gain parametric down conversion," Laser Phys. Lett. **12**, 065202 (2015).
23. L. Yang, F. Sun, N. Zhao, and X. Li, "Generation of frequency degenerate twin photons in pulse pumped fiber optical parametric amplifiers: Influence of background noise," Opt. Express **22**, 2553–2561 (2014).
24. B. Yurke and M. Potasek, "Obtainment of thermal noise from a pure quantum state," Phys. Rev. A **36**, 3464–3466 (1987).
25. A. Christ, K. Laiho, A. Eckstein, K. N. Cassemiro, and C. Silberhorn, "Probing multimode squeezing with correlation functions," New J. Phys. **13**, 033027 (2011).
26. X. Guo, X. Li, N. Liu, and Z. Y. Ou, "Multi-mode theory of generating pulsed twin beams from a high gain fiber optical parametric amplifier," Phys. Rev. A **88**, 023841 (2013).
27. O. Alibart, J. Fulconis, G. K. L. Wong, S. G. Murdoch, W. J. Wadsworth, and J. G. Rarity, "Photon pair generation using four-wave mixing in a microstructured fibre: theory versus experiment," New J. Phys. **8**, 67 (2006).
28. X. Li, X. Ma, Z. Y. Ou, L. Yang, L. Cui, and D. Yu, "Spectral study of photon pairs generated in dispersion shifted fiber with a pulsed pump," Opt. Express **16**, 32–44 (2008).
29. L. Cui, X. Li, and N. Zhao, "Minimizing the frequency correlation of photon pairs in photonic crystal fibers," New J. Phys. **14**, 123001 (2012).
30. C. K. Law, I. A. Walmsley, and J. H. Eberly, "Continuous frequency entanglement: effective finite hilbert space and entropy control," Phys. Rev. Lett **84**, 5304–5307 (2000).
31. M. Avenhaus, K. Laiho, M. V. Chekhova, and C. Silberhorn, "Accessing higher order correlations in quantum optical states by time multiplexing," Phys. Rev. Lett **104**, 063602 (2010).
32. M. Liscidini and J. E. Sipe, "Stimulated emission tomography," Phys. Rev. Lett. **111**, 193602 (2013).
33. A. Eckstein, G. Boucher, A. Lemaître, P. Filloux, I. Favero, G. Leo, J. E. Sipe, M. Liscidini, and S. Ducci, "High-resolution spectral characterization of two photon states via classical measurements," Laser Photonics Rev. **8**, L76–L80 (2014).
34. X. Li, J. Chen, P. Voss, J. Sharping, and P. Kumar, "All-fiber photon-pair source for quantum communications: Improved generation of correlated photons," Opt. Express **12**, 3737–3744 (2004).
35. S. Gerke, J. Sperling, W. Vogel, Y. Cai, J. Roslund, N. Treps, and C. Fabre, "Full multipartite entanglement of

#253936 Received 16 Nov 2015; revised 20 Dec 2015; accepted 5 Jan 2016; published 13 Jan 2016

1. Introduction

Pulse-pumped, single pass spontaneous parametric emission, including $\chi^{(2)}$ nonlinearity based spontaneous parametric down-conversion (SPDC) and $\chi^{(3)}$ nonlinearity based spontaneous four-wave mixing (SFWM), is one of the most popular approaches for generating the quantum states of light [1–7]. Because of the broadband nature of the pulsed pump field, there does not exist well-defined frequency correlation between the signal and the idler fields produced by the SPDC and SFWM. So the temporal/spectral properties of the signal and idler twin beams are quite complicated [8]. So far, the temporal properties of signal and idler twin beams generated by a pulse-pumped SPDC and SFWM in the low gain regime have been extensively studied [9–11], because it affects the visibility of the Hong-Ou-Mandel interference between independent sources, which plays an important role for fulfilling quantum information processing (QIP) tasks, such as quantum teleportation, entanglement swapping, and linear optical quantum computing etc. [12–14]. On the other hand, the pulse-pumped SPDC and SFWM in the high gain regime can be used to generate continuous variable (CV) quantum lights, such as multimode squeezed state and Einstein-Podolsky-Rosen (EPR) entangled state [1, 4, 5, 15, 16], which are important resources for quantum simulation and quantum metrology [17]. It has been understood that matching the temporal modes between the twin beams and local oscillators of the homodyne detection system is critical for improving the quality of the multimode quantum light [5, 16]. Therefore, it is necessary to make a detailed analysis of the temporal properties of twin beams.

Recently, there are a series of experimental investigations on the spatial and temporal properties of twin beams generated by the high gain SPDC in bulk $\chi^{(2)}$ crystals [18–22]. However, the results are affected by the complicated interplay of both the spatial and temporal modes because ultrashort pump pulses are employed to achieve high gain. In this paper, we exclude the influence of the spatial mode by exploiting single spatial mode optical fiber for the generation of the twin beams via the high gain SFWM [2, 23]. Because the individual signal/idler beam is in thermal state, the temporal properties are related to the intensity correlation function $g^{(2)}$ when the response time of detectors is much longer than the pulse duration of twin beams [8, 22, 24, 25]. We may therefore characterize the temporal mode properties of the signal and idler beams by measuring the $g^{(2)}$ under different setting of the experimental parameters.

The rest of the paper is organized as follows. In Sec. II, we theoretically analyze the temporal property of twin beams by deducing the general expression of $g^{(2)}$ and numerically calculating $g^{(2)}$ of individual signal/idler beam under different conditions. Our analysis is based on our previous work [16] with the method of singular value decomposition. This approach was recently employed for spatial mode analysis in high gain bulk $\chi^{(2)}$ parametric down-conversion processes [21, 22]. The results show that the temporal property depends not only on the phase matching condition and the bandwidth of the filters applied in signal and idler bands, but also on the gain of SFWM. In Sec. III, we present the experimental verification using the twin beams generated by the pulse-pumped SFWM in a piece of dispersion shifted fiber (DSF). The results show that the measured $g^{(2)}$ is in consistent with the theoretical expectation and we achieve near single temporal mode operation in twin beams generation. Finally, we end with a brief summary in Sec. IV.

2. Theoretical analysis

The conceptual representation of the scheme for studying the spectral properties of the signal and idler twin beams generated from the high gain SFWM is shown in Fig. 1. The SFWM is

#253936 Received 16 Nov 2015; revised 20 Dec 2015; accepted 5 Jan 2016; published 13 Jan 2016

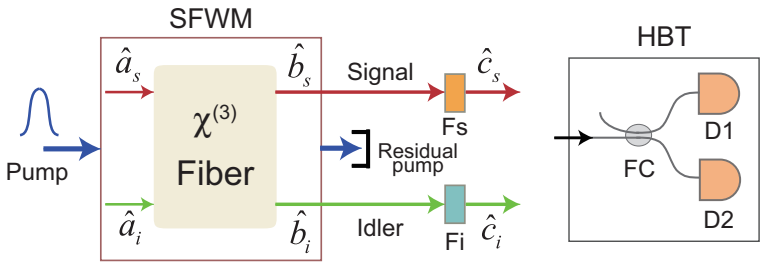

Fig. 1. Conceptual representation of the scheme for generating the twin beams via SFWM in fiber and the Hanbury Brown-Twiss (HBT) interferometer for measuring the intensity correlation function of individual signal (idler) beam $g^{(2)}_{s(i)}$. $F_{s(i)}$, filter in signal (idler) band; FC, fiber coupler; D1-D2, detector.

realized by launching pulsed pump field into a nonlinear fiber, which satisfies the required phase matching condition. In the SFWM process, two pump photons at angular frequency ω_p are coupled via $\chi^{(3)}$ of the nonlinear fiber to simultaneously create a pair of signal and idler photons at frequencies ω_s and ω_i, respectively, with the energy conservation relation $2\omega_p = \omega_s + \omega_i$. At the output port of the nonlinear fiber, the filters F_s and F_i are applied to reject the pump field and to separate the signal and idler fields. We analyze the spectral property by measuring the normalized intensity correlation function $g^{(2)}_s$ ($g^{(2)}_i$) of individual signal (idler) field. To do so, the filtered signal/idler field is sent into a Hanbury Brown-Twiss (HBT) interferometer, consisting of a 50/50 fiber coupler (FC) and two detectors (D1 and D2).

The theoretical model for the SFWM process in a nonlinear fiber was described in detail in [16] and [26]. Before evaluating the normalized correlation function, let us first present those results that are related to the current paper.

The strong pump pulses propagating along the fiber are described by a transform limited pulsed laser with a Gaussian shaped spectrum:

$$E_p(t) = E_0 e^{-i\gamma P_p z} \int e^{-\frac{(\omega_p-\omega_{p0})^2}{2\sigma_p^2}} e^{i(k_p z-\omega_p t)} d\omega_p, \tag{1}$$

where σ_p, ω_{p0} and k_p are the bandwidth, central frequency, and wave vector of the pump field, respectively, and E_0 is related to the peak power through the relation $P_p = 2\pi\sigma_p^2 E_0^2$. The term $e^{-i\gamma P_p z}$ is originated from the self-phase modulation with γ denoting the nonlinear coefficient of the fiber. The quantized one-dimensional negative-frequency field operators

$$\hat{E}_s^{(-)}(t) = \frac{1}{\sqrt{2\pi}} \int d\omega_s' \hat{a}_s^\dagger(\omega_s') e^{-i(k_s z-\omega_s' t)} \tag{2a}$$

and

$$\hat{E}_i^{(-)}(t) = \frac{1}{\sqrt{2\pi}} \int d\omega_i' \hat{a}_i^\dagger(\omega_i') e^{-i(k_i z-\omega_i' t)} \tag{2b}$$

respectively describe the inputs of signal and idler fields. The output signal (idler) field $\hat{b}_{s(i)}(\omega_{s(i)})$ is a superposition of many amplified input signal and idler frequency modes $\hat{a}_s(\omega_s)$ and $\hat{a}_i(\omega_i)$. The general input-output relationships of the operators are written as:

$$\hat{b}_s(\omega_s) = \hat{U}^\dagger \hat{a}_s(\omega_s)\hat{U} = \int_S h_{1s}(\omega_s,\omega_s')\hat{a}_s(\omega_s')d\omega_s' + \int_I h_{2s}(\omega_s,\omega_i')\hat{a}_i^\dagger(\omega_i')d\omega_i' \tag{3a}$$

$$\hat{b}_i(\omega_i) = \hat{U}^\dagger \hat{a}_i(\omega_i)\hat{U} = \int_I h_{1i}(\omega_i,\omega_i')\hat{a}_i(\omega_i')d\omega_i' + \int_S h_{2i}(\omega_i,\omega_s')\hat{a}_s^\dagger(\omega_s')d\omega_s', \tag{3b}$$

#253936 Received 16 Nov 2015; revised 20 Dec 2015; accepted 5 Jan 2016; published 13 Jan 2016

where S and I respectively represent the integration frequency range of the signal and idler fields, and the functions $h_{1s}, h_{2s}, h_{1i}, h_{2i}$ are referred to as Green functions. The operators of the input and output signal (idler) fields satisfy the commutation relation $[\hat{a}_{s(i)}(\omega'_{s(i)1}), \hat{a}^{\dagger}_{s(i)}(\omega'_{s(i)2})] = \delta(\omega'_{s(i)1} - \omega'_{s(i)2})$ and $[\hat{b}_{s(i)}(\omega_{s(i)1}), \hat{b}^{\dagger}_{s(i)}(\omega_{s(i)2})] = \delta(\omega_{s(i)1} - \omega_{s(i)2})$, respectively. The unitary evolution operator $\hat{U}$ is given by

$$\hat{U} = \exp\left\{ G\big[\iint F(\omega'_s, \omega'_i)\hat{a}^{\dagger}_s(\omega'_s)\hat{a}^{\dagger}_i(\omega'_i)d\omega'_s d\omega'_i - h.c.\big] \right\}, \tag{4}$$

where $G \propto \gamma P_p L$ is the gain coefficient of SFWM, and

$$F(\omega_s, \omega_i) = \frac{C_N}{2\sqrt{\pi}\sigma_p} \exp\left[\frac{-(\omega_s + \omega_i - 2\omega_{p0})^2}{4\sigma_p^2} \right] \mathrm{sinc}\left(\frac{\Delta k L}{2} \right) \tag{5}$$

is the joint spectrum function (JSF) with C_N denoting a constant to ensure the normalization condition $\iint |F(\omega_s, \omega_i)|^2 d\omega_s d\omega_i = 1$. Here $\Delta k = k_s + k_i - 2k_p + 2\gamma P_p$ with $k_{s(i)}$ denoting the wave vector of signal (idler) field is the phase mismatching term. Using the Taylor expansion of k_p, k_s, and k_i at the perfect phase matching frequencies, ω_{p0}, ω_{s0} and ω_{i0}, respectively, and balancing out the self-phase modulation term $2\gamma P_p$ for optimum phase matching [27–29], we get

$$\Delta k \approx \frac{\Omega_s}{A} + \frac{\Omega_i}{B}, \tag{6}$$

where A, B are determined by the dispersion coefficients of the nonlinear fiber, and $\Omega_{s(i)}$ is related to $\omega_{s0(i0)}$ by $\Omega_{s(i)} = \omega_{s(i)} - \omega_{s0(i0)}$.

The JSF is referred to as the probability amplitude of simultaneously finding a pair of signal and idler photons within the frequency range of $\omega_s \to \omega_s + d\omega_s$ and $\omega_i \to \omega_i + d\omega_i$, respectively. According to [16], we can make a singular-value decomposition (SVD) (also known as Schmidt decomposition [30]) of the JSF as

$$F(\omega_s, \omega_i) = \sum_k r_k \phi_k(\omega_s)\psi_k(\omega_i) \qquad \big(k = 1, 2, ...\big), \tag{7}$$

where the complex functions $\phi_k(\omega_s)$ and $\psi_k(\omega_i)$, satisfying the orthonormal relations

$$\begin{aligned} \int \phi^*_{k1}(\omega_s)\phi_{k2}(\omega_s)d\omega_s &= \delta_{k1,k2}, \\ \int \psi^*_{k1}(\omega_i)\psi_{k2}(\omega_i)d\omega_i &= \delta_{k1,k2}, \end{aligned} \tag{8}$$

represent the spectrum of signal and idler fields in the kth order temporal mode, and the real eigenvalue $r_k \geq 0$, satisfying the normalization condition $\sum_k |r_k|^2 = 1$, is referred to as the mode amplitude. For the sake of clarity, the mode index k are arranged in a descending order, so that the mode amplitudes satisfy $r_{k-1} \geq r_k \geq r_{k+1} \cdots$ for $k \geq 2$. For the case of $k = 1$, the functions $\phi_1(\omega_s)$ and $\psi_1(\omega_i)$ are referred to as the fundamental modes.

With the SVD, the Green functions in Eq. (3) are related to $\phi_k(\omega_s), \psi_k(\omega_i), r_k$ and the gain coefficient G in a series expansion form

$$h_{1s}(\omega_s, \omega'_s) = \delta(\omega_s - \omega'_s) + \sum_k [\cosh(r_k G) - 1]\phi_k(\omega_s)\phi^*_k(\omega'_s) \tag{9}$$

$$h_{2s}(\omega_s, \omega'_i) = \sum_k \sinh(r_k G)\phi_k(\omega_s)\psi_k(\omega'_i) \tag{10}$$

$$h_{1i}(\omega_i, \omega'_i) = \delta(\omega_i - \omega'_i) + \sum_k [\cosh(r_k G) - 1]\psi_k(\omega_i)\psi^*_k(\omega'_i) \tag{11}$$

$$h_{2i}(\omega_i, \omega'_s) = \sum_k \sinh(r_k G)\psi_k(\omega_i)\phi_k(\omega'_s). \tag{12}$$

#253936 Received 16 Nov 2015; revised 20 Dec 2015; accepted 5 Jan 2016; published 13 Jan 2016

In the HBT interferometer, the operator of the signal (idler) field propagating through the filter is expressed as

$$\hat{c}_{s(i)}(\omega_{s(i)}) = \sqrt{\eta_{s(i)}} f(\omega_{s(i)}) \hat{b}_{s(i)}(\omega_{s(i)}) + \sqrt{1-\eta_{s(i)} f^2(\omega_{s(i)})} \hat{v}_{s(i)}(\omega_{s(i)}) \tag{13}$$

where $\eta_{s(i)}$ and Gaussian function $f(\omega_{s(i)}) = \exp[-\frac{(\omega_{s(i)}-\omega_{s0(i0)})^2}{2\sigma^2_{s(i)}}]$ with $\sigma_{s(i)}$ denoting the bandwidth are referred to as the transmission efficiency and spectrum of the filter F_s (F_i) in signal (idler) band, respectively, and $\hat{v}_{s(i)}(\omega_{s(i)})$ is the annihilation operator for the vacuum mode added to model the loss. After passing the signal (idler) field through the 50/50 FC, the electric-fields respectively incident on the detectors D1 and D2 are written as

$$E^{(-)}_{D1}(t) = \frac{\sqrt{\eta_{D1}}}{2\sqrt{\pi}} \int d\omega_{s(i)} c^{\dagger}_{s(i)}(\omega_{s(i)}) e^{-i(k_{s(i)}z-\omega_{s(i)}t)} + \frac{\sqrt{1-\eta_{D1}}}{2\sqrt{\pi}} \int d\omega_{s(i)} v^{\dagger}_{s(i)}(\omega_{s(i)}) e^{-i(k_{s(i)}z-\omega_{s(i)}t)} \tag{14a}$$

$$E^{(-)}_{D2}(t) = \frac{\sqrt{\eta_{D2}}}{2\sqrt{\pi}} \int d\omega_{s(i)} c^{\dagger}_{s(i)}(\omega_{s(i)}) e^{-i(k_{s(i)}z-\omega_{s(i)}t)} + \frac{\sqrt{1-\eta_{D2}}}{2\sqrt{\pi}} \int d\omega_{s(i)} v^{\dagger}_{s(i)}(\omega_{s(i)}) e^{-i(k_{s(i)}z-\omega_{s(i)}t)}, \tag{14b}$$

where $\eta_{D1(2)}$ is the quantum efficiency of D1 (D2). Accordingly, the normalized intensity correlation function measured by the two detectors is written as

$$g^{(2)} = \frac{\int dt_1 dt_2 \left\langle 0 \left| E^-_{D1}(t_1) E^-_{D2}(t_2) E^+_{D2}(t_2) E^+_{D1}(t_1) \right| 0 \right\rangle}{\int dt_1 \left\langle 0 \left| E^-_{D1}(t_1) E^+_{D1}(t_1) \right| 0 \right\rangle \int dt_2 \left\langle 0 \left| E^-_{D2}(t_2) E^+_{D2}(t_2) \right| 0 \right\rangle}. \tag{15}$$

With the response time of each detector much longer than the creation time period of signal and idler photons, which are confined within the pump pulse duration, the time integral can be treated as an integral from $-\infty$ to $+\infty$ [25]. By substituting Eqs. (13) and (14) into Eq. (15), $g^{(2)}$ of signal/idler beam can be calculated and expressed as

$$g^{(2)}_{s(i)} = 1 + \frac{\mathscr{E}_{s(i)}}{\mathscr{A}_{s(i)}} \tag{16}$$

with

$$\begin{aligned} \mathscr{E}_{s(i)} &\equiv \int d\omega_{s(i)} d\omega'_{s(i)} d\omega'_1 d\omega'_2 |f_{s(i)}(\omega_{s(i)})|^2 |f_{s(i)}(\omega'_{s(i)})|^2 \\ &\quad \times h^*_{2s(i)}(\omega_{s(i)}, \omega'_2) h^*_{2s(i)}(\omega'_{s(i)}, \omega'_1) h_{2s(i)}(\omega'_{s(i)}, \omega'_2) h_{2s(i)}(\omega_{s(i)}, \omega'_1), \end{aligned} \tag{17}$$

$$\mathscr{A}_{s(i)} \equiv \left[\int d\omega_{s(i)} d\omega' \left| f_{s(i)}(\omega_{s(i)}) h_{2s(i)}(\omega_{s(i)}, \omega') \right|^2 \right]^2. \tag{18}$$

Equations (16)-(18) show that $g^{(2)}_{s(i)}$ is related to the filter function $f_{s(i)}(\omega_{s(i)})$ and the Green function $h_{2s(i)}(\omega_{s(i)}, \omega_{i(s)})$, but is independent upon the transmission efficiency and detection efficiency [25, 31]. Substituting above with Eqs. (10,12) and orthonormal relations in Eq. (8), we obtain

$$\mathscr{E}_{s(i)} = \sum_{k_1,k_2} \sinh^2(r_{k_1} G) \sinh^2(r_{k_2} G) \left| \Delta^{s(i)}_{k_1 k_2} \right|^2, \tag{19}$$

$$\mathscr{A}_{s(i)} = \sum_{k_1,k_2} \sinh^2(r_{k_1} G) \sinh^2(r_{k_2} G) \Delta^{s(i)}_{k_1 k_1} \Delta^{s(i)}_{k_2 k_2} \tag{20}$$

with

$$\Delta^{s}_{k_1 k_2} \equiv \int d\omega_s |f_s(\omega_s)|^2 \phi^*_{k_1}(\omega_s) \phi_{k_2}(\omega_s),$$

#253936 Received 16 Nov 2015; revised 20 Dec 2015; accepted 5 Jan 2016; published 13 Jan 2016

$$\Delta^{i}_{k_1k_2} \equiv \int d\omega_s |f_i(\omega_i)|^2 \psi^*_{k_1}(\omega_i)\psi_{k_2}(\omega_i). \quad (21)$$

Cauchy-Schwarz inequality gives $\Delta^{s(i)}_{k_1k_1}\Delta^{s(i)}_{k_2k_2} \geq \left|\Delta^{s(i)}_{k_1k_2}\right|^2$ so that $\mathscr{A} \geq \mathscr{E} \geq 0$ and $1 \leq g^{(2)} \leq 2$. When there is no optical filtering, i.e., $f_s(\omega_s) = 1 = f_i(\omega_i)$, we have $\Delta^{s}_{k_1k_2} = \Delta^{i}_{k_1k_2} = \delta_{k_1k_2}$ and

$$\mathscr{E}_{s(i)} = \sum_k \sinh^4(r_kG), \quad (22)$$

$$\mathscr{A}_{s(i)} = \left[\sum_k \sinh^2(r_kG)\right]^2. \quad (23)$$

Moreover, by defining the coefficient $\lambda_k = \frac{\sinh(r_kG)}{\sqrt{\sum_k \sinh^2(r_kG)}}$ ($\sum_k |\lambda_k|^2 = 1$), which denotes the normalized amplitude of the kth order mode of amplified signal and idler twin beams, Eq. (16) can be rewritten as

$$g^{(2)} = 1 + \sum_k \lambda_k^4. \quad (24)$$

The equation above was also derived by Christ et al [25] and by Sharopova et al [21] and Dyakonov et al [22] for spatial mode analysis in high gain parametric down-conversion.

If there are M modes with nearly equal mode amplitudes: $r_k = r$ ($k = 1,...,M$) or $\lambda_k = \lambda$ ($k = 1,...,M$), then $\mathscr{E}/\mathscr{A} = 1/M$ and $g^{(2)} = 1 + \frac{1}{M}$. For single-mode case of $r_1 = 1,\ r_k = 0 (k \neq 1)$ or $\lambda_1 = 1,\ \lambda_k = 0 (k \neq 1)$, we always have $g^{(2)} = 2$.

At low gain of $G \ll 1$, we have

$$g^{(2)} \approx 1 + \sum_k r_k^4. \quad (25)$$

But at high gain of $G \gg 1$, we have

$$g^{(2)} = 1 + \frac{1 + \sum_{k\neq 1} \nu_k^2}{[1 + \sum_{k\neq 1} \nu_k]^2} \quad (26)$$

with $\nu_k \equiv \lambda_k^2/\lambda_1^2 = \sinh^2(r_kG)/\sinh^2(r_1G) \approx e^{-2(r_1-r_k)G} \leq e^{-2(r_1-r_2)G} \ll 1$ for $G \gg 1/(r_1 - r_2)$. In this case, Eq. (26) becomes

$$g^{(2)} \approx 2\Big(1 - \sum_{k\neq 1} \nu_k\Big). \quad (27)$$

Here, we dropped higher order terms in ν_k. So, $g^{(2)} \to 2$ for $G \gg 1/(r_1 - r_2)$.

From the way that $g^{(2)} \to 2$ as G becomes large, we find that the contribution from the fundamental mode of $k = 1$ dominates at large G so that the generated field can be effectively considered as a single-mode field, even though the field is of multi-mode nature at low gain. Another way to achieve single-mode operation and $g^{(2)} \to 2$ is optical filtering. From the expression for $\mathscr{E}, \mathscr{A}$ in Eqs. (19) and (20) and for $\Delta^{s(i)}_{k_1k_2}$ in Eq. (21), we find that we can narrow the bandwidth of $f_{s(i)}(\omega_{s(i)})$ so that it is much smaller than that of $\phi_k(\omega), \psi_k(\omega)$. Then, $\Delta^{s(i)}_{k_1k_2} \approx C^{s(i)*}_{k_1} C^{s(i)}_{k_2}$ ($C^{s}_{kn} = \phi_{kn}(0)\sqrt{\int d\omega_s |f_s(\omega_s)|^2}$, $C^{i}_{kn} = \psi_{kn}(0)\sqrt{\int d\omega_i |f_i(\omega_i)|^2}$, $n = 1,2$), which is factorized and leads to $\Delta^{s(i)}_{k_1k_1}\Delta^{s(i)}_{k_2k_2} \approx \left|\Delta^{s(i)}_{k_1k_2}\right|^2$ or $\mathscr{E} \approx \mathscr{A}$ and $g^{(2)} \approx 2$. In the following, we will consider some numerical simulations to visualize how $g^{(2)}$ approaches to 2 as we change the gain and the filter bandwidth.

#253936 Received 16 Nov 2015; revised 20 Dec 2015; accepted 5 Jan 2016; published 13 Jan 2016

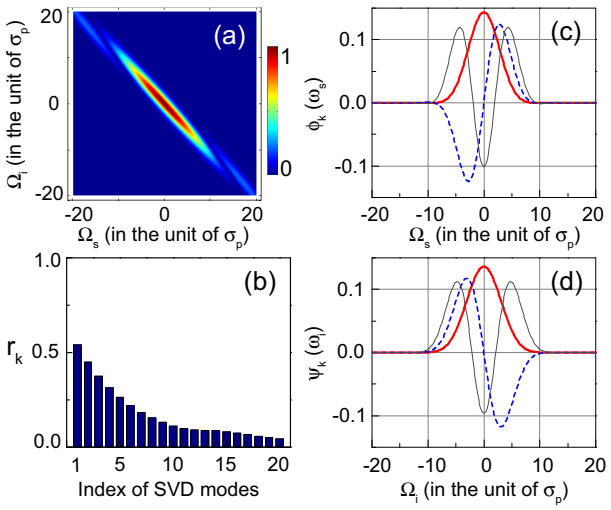

Fig. 2. (a) The normalized contour map of JSF $|F(\omega_s,\omega_i)/F(\omega_{s0},\omega_{i0})|$ and (b) the corresponding amplitude of the kth order decomposed mode r_k. (c) and (d) are the spectra of the first three decomposed modes in signal and idler fields ($k=1,2,3$), respectively. The red, blue and grey curves are for the mode with index $k=1$, $k=2$, and $k=3$, respectively. In the simulation, we have $\Delta k=\frac{\Omega_s}{0.6\sigma_p L}+\frac{\Omega_i}{0.9\sigma_p L}$ in Eq. (5).

As an example, we analyze the normalized JSF $|F(\omega_s,\omega_i)/F(\omega_{s0},\omega_{i0})|$ when the phase mismatch term in Eq. (5) is $\Delta k=\frac{\Omega_s}{0.6\sigma_p L}+\frac{\Omega_i}{0.9\sigma_p L}$. In the calculation, all the frequency scales are in the unit of the pump bandwidth σ_p. The result in Fig. 2(a) illustrates that the frequencies of the signal and idler photon pairs generated by low gain SFWM is highly anti-correlated. Figure 2(b) plots the corresponding amplitude of the decomposed kth order modes, $\phi_k(\omega_s)$ and $\psi_k(\omega_i)$. It is clear that the amplitude r_k gradually decrease with the increase of mode index k, and cannot be neglected for the case of $k<15$.

Moreover, since Eqs. (16)-(18) illustrate that the spectral property of twin beams is directly related to the Green function $h_{2s(i)}(\omega_{s(i)},\omega_{i(s)})$, rather than the JSF, we then calculate the contour map of normalized $h_{2s(i)}(\omega_{s(i)},\omega_{i(s)})$ and the normalized amplitude of the kth order mode λ_k as a function of the gain coefficient G. The calculation shows that the normalized Green functions of the signal and idler beams $|h_{2s}(\omega_s,\omega_i)/h_{2s}(\omega_{s0},\omega_{i0})|$ and $|h_{2i}(\omega_i,\omega_s)/h_{2i}(\omega_{i0},\omega_{s0})|$ have the same pattern. As shown in Fig. 3, in the low gain regime ($G=0.1$), we have $h_{2s(i)}(\omega_{s(i)},\omega_{i(s)})\propto F(\omega_s,\omega_i)$; with the increase of G, the corresponding amplitude of the fundamental mode λ_1 increases. For the case of $G=20$, we have $\lambda_1\to 1$. The results indicate the factorability of $h_{2s(i)}(\omega_{s(i)},\omega_{i(s)})$ increase with G, and it can be written into a factorized form $h_{2s(i)}(\omega_{s(i)},\omega_{i(s)})\approx\phi(\omega_s)*\psi(\omega_i)$ in the high gain limit.

Figure 4 shows the value of $g^{(2)}_{s(i)}$ calculated by varying the gain coefficient and the filter bandwidth. In the calculation, the JSF is the same as Fig. 2, and the bandwidth of the filter in Eqs. (16)-(18) is $\sigma_{s(i)}=R\sigma_p$ in signal (idler) field with $R=1,2,3$ and $R\to\infty$ ($f_s(\omega_s)=1=f_i(\omega_i)$). One sees that for a fixed gain coefficient G, particularly in the low gain regime, $g^{(2)}_{s(i)}$ increases with the decrease of R because the average mode number decrease with the bandwidth of thermal field; while for the fixed filter bandwidth ratio $R=\sigma_{s(i)}/\sigma_p$, $g^{(2)}_{s(i)}$ increases with G and approaches to 2 in the high gain limit. The result indicates that using criterion of $g^{(2)}_{s(i)}\to 2$

#253936 Received 16 Nov 2015; revised 20 Dec 2015; accepted 5 Jan 2016; published 13 Jan 2016

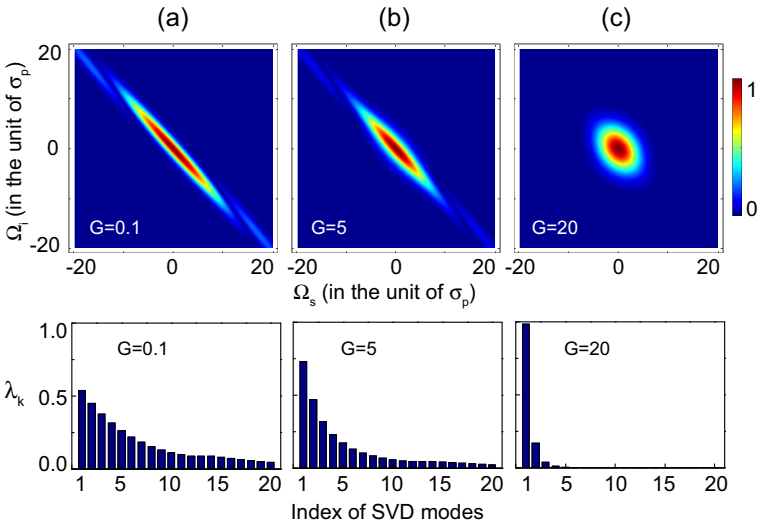

Fig. 3. The normalized Green function $|h_{2s(i)}(\omega_{s(i)},\omega_{i(s)})/h_{2s(i)}(\omega_{s0(i0)},\omega_{i0(s0)})|$ and the normalized amplitude of the kth order mode $\lambda_k = \frac{\sinh(r_k G)}{\sqrt{\sum_k \sinh^2(r_k G)}}$ for the gain coefficient of (a) $G = 0.1$, (b) $G = 5$ and (c) $G = 20$, respectively. In the calculation, the JSF is the same as Fig. 2.

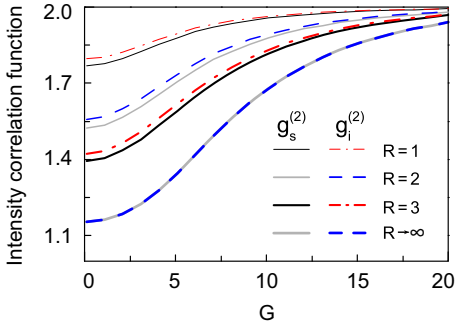

Fig. 4. Intensity correlation function of individual signal and idler beams, $g_s^{(2)}$ and $g_i^{(2)}$, versus G for filter with different ratio $R = \sigma_{s(i)}/\sigma_p$. $R \to \infty$ is equivalent to no filter is applied in signal (idler) band, i.e., $f_s(\omega_s) = 1 = f_i(\omega_i)$. In the calculation, the JSF is the same as Fig. 2.

to characterize the factorability of JSF is not valid unless the gain of SPDC or SFWM is low enough [32, 33]. Additionally, we find that for the fixed parameters of gain and filter, G and R, $g_i^{(2)}$ is slightly higher than $g_s^{(2)}$. We believe this is caused by the asymmetry of JSF in Fig. 2. Although the mode numbers of signal and idler fields are the same when no filter ($R \to \infty$) is applied at the output of nonlinear fiber, the frequency distribution of the kth mode for signal field $\phi_k(\omega_s)$ is slightly narrower than that for idler field $\psi_k(\omega_i)$, as illustrated by the spectral function of first three decomposed modes in Figs. 2(c) and 2(d). Therefore, for the filters with same bandwidth in signal and idler channels, the average mode number of the filtered signal field is larger than that of the filtered idler field.

#253936 Received 16 Nov 2015; revised 20 Dec 2015; accepted 5 Jan 2016; published 13 Jan 2016

3. Experiment

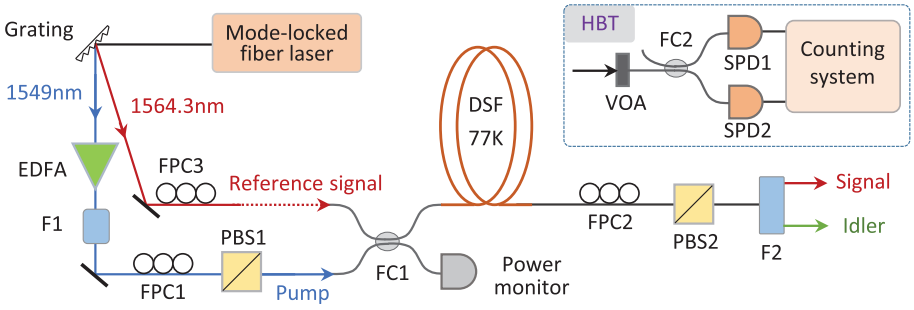

Fig. 5. Experimental setup. DSF: dispersion shift fiber; EDFA: erbium-doped fiber amplifier; F1-F2: filter; FC1: 90/10 fiber coupler; FC2: 50/50 fiber coupler; FPC1-FPC3: fiber polarization controller; PBS1-PBS2: polarization beam splitter; VOA: variable optical attenuator; SPD1-SPD2: single photon detector.

Figure 5 is the experimental setup exploited to verify our theoretical analysis. High gain SFWM is realized by pumping 300 m DSF with strong laser pulses. The 90/10 fiber coupler (FC1) is used not only for splitting 10% of the pump as a power monitor, but also for characterizing the gain of SFWM by coupling 90% of the pump and 10% of the reference signal pulses into the DSF. The nonlinear coefficient and zero dispersion wavelength (ZDW) of the DSF submerged in liquid nitrogen are about 2 W^{-1}/km and 1548 nm, respectively. During the measurement of $g^{(2)}_{s(i)}$, the reference signal light is blocked.

We create the pump and reference signal pulses by taking a 36 MHz train of 100-fs pulses centered at 1550 nm from a mode-locked fiber laser, dispersing them with a grating and then spectrally filtering them to obtain two synchronous beams with central wavelengths of about 1549 and 1564.3 nm, respectively. This arrangement gives the nearly transform-limited pump and reference signal with pulse duration of about 4 and 3 ps, respectively. To achieve the required pump power, the pump pulses are then amplified by an erbium-doped fiber amplifier (EDFA), and further cleaned up with a bandpass filter F1 having central wavelength and full width at half maximum (FWHM) of about 1549 and 0.8 nm, respectively. The polarization and power of the pump are controlled by a fiber polarization controller (FPC1) and a fiber polarization beam splitter (PBS1). Under this condition, the co-polarized SFWM with a broad gain bandwidth is phase matched in DSF, so the reference signal centering at 1564.3 nm can be significantly amplified by co-propagating with the pump through DSF.

The signal and idler fields co-polarized with the pump are selected by adjusting FPC2 placed in front of PBS2. Dual-band filter F2, whose central wavelengths in the signal and idler bands are 1564.3 and 1534 nm, respectively, is used to suppress the pump field and to separate signal and idler fields. The pump-rejection ratio of F2, realized by cascading two coarse wavelength division multiplexing (CWDM) filters with a wave shaper (Finisar Waveshaper 4000S), is in excess of 120 dB. The FWHM of F2 in signal and idler bands can be adjusted by properly setting the wave shaper.

We first characterize the high gain feature of SFWM. In the experiment, the temporal and polarization modes of reference signal and pump are well matched by adjusting the path length of reference signal and FPC3, respectively. A power meter is placed at the signal channel of F2, whose bandwidth is adjusted to much broader than the reference light. When the power of the injected reference signal is $I_{in} = 1\ \mu W$, we measure the power of amplified signal I_{out} by varying the pump power. Figure 6(a) plots the measured power gain $g = I_{out}/I_{in}$ versus pump

#253936 Received 16 Nov 2015; revised 20 Dec 2015; accepted 5 Jan 2016; published 13 Jan 2016

power. One sees that $g = 60$ is obtained for the pump with average power of about 2 mW.

To evaluate the gain coefficient G, we decompose the normalized Gaussian spectrum of the reference signal $S(\omega_s) = \frac{1}{\sqrt{\sqrt{\pi}\sigma_{si}}} \exp[-\frac{(\omega_s-\omega_0)^2}{2\sigma_{s1}^2}]$ in the base of signal modes:

$$S(\omega_s) = \sum_k \xi_{sk}\phi_k(\omega_s). \tag{28}$$

The measured power gain can be viewed as the sum of the gain of each decomposed SVD mode nonorthogonal to the mode of the reference signal, i.e.,

$$g = \sum_k |\xi_{sk}|^2 \cosh^2(r_k G), \tag{29}$$

where the complex coefficient ξ_{sk} characterizes the mode matching efficiency between the reference signal and the decomposed kth order mode [16], and $\cosh^2(r_k G)$ is the power gain of the kth order mode $\phi_k(\omega_s)$. According to the normalization condition $\sum_k |\xi_{sk}|^2 = 1$ and the JSF deduced from the dispersion property of the DSF [28], we find the gain coefficient G is about 5.2 for $g = 60$. It should be mentioned that this is a rough estimation of the gain coefficient G since the JSF actually depends on the pump power due to self-phase modulation and so do the mode function $\phi_k(\omega_s)$ in Eq.(28) (see later for detail).

We then characterize the spectral property of the individual signal (idler) beam by measuring its intensity correlation function $g^{(2)}_{s(i)}$. Since the value of $g^{(2)}_{s(i)}$ is independent on the transmission and detection efficiency (see Eqs. (16)-(18)), we heavily attenuate the signal (idler) field to single photon level by the variable optical attenuator (VOA). For the measurement fulfilled by the HBT interferometer, the attenuated signal (idler) field is fed to the input port of 50/50 FC (FC2), and the two outputs of FC2 are detected by single photon detectors (SPD, id200) SPD1 and SPD2, respectively. The two SPDs are operated in the gated Geiger mode. The 2.5-ns gate pulses of SPDs arrive at a rate of about 3.6 MHz, which is 1/10 of the repetition rate of the pump pulses, and the dead time of the gate is set to be 10 μs.

During the measurement, we record both the coincidence and accidental coincidence of two SPDs, which are obtained by detecting signal (idler) photons originated from the same and adjacent pump pulses, respectively. The normalized intensity correlation function $g^{(2)}_{s(i)}$ is the ratio between the measured coincidence and accidental coincidence rates. Figures 6(b) and 6(c) show the measured $g^{(2)}_s$ and $g^{(2)}_i$ as a function of the average pump power when the ratio $R = \sigma_{s(i)}/\sigma_p$ is 1, 2 and 3, respectively. One sees that the measured $g^{(2)}_{s(i)}$ is distinctly less than 2 in the low gain regime even if the narrow band filter is applied due to the anti-frequency correlation of the JSF in DSF [28]. However, $g^{(2)}_{s(i)}$ increases with pump power for each setting of R, and the trend is more obvious for the cases of $R = 2$ and $R = 3$. Comparing Figs. 6(b) and 6(c), one sees that for a fixed ratio R, $g^{(2)}_i$ is slightly larger than $g^{(2)}_s$, because the JSF of the photon pairs generated in the DSF is asymmetric [28] (similar to Fig. 2(a)). Notice that the highest value of $g^{(2)}$ is 1.97 ± 0.02, indicating a near single temporal mode situation.

We note that the spontaneous Raman scattering (RS) will accompany the SFWM process in DSF [34]. However, in our experiment, the gain of RS at the wavelength of signal and idler beams is very low. For example, for the average pump power of about 0.45 mW, when the detection rate of photons via SFWM is about 2.9×10^{-3} photons/pulse/nm, the rate of photons via RS is only about 0.17×10^{-3} photons/pulse/nm. Therefore, the detected photons originated from SFWM is at least 17 times greater than that originated from RS. Since the intensity of RS lineally depends on pump power [34], but the intensity of photons via SFWM exponentially depends on the peak power of pump in high gain regime (see Fig. 6(a)), the influence of RS on the measurement of $g^{(2)}_{s(i)}$ can be ignored.

#253936 Received 16 Nov 2015; revised 20 Dec 2015; accepted 5 Jan 2016; published 13 Jan 2016

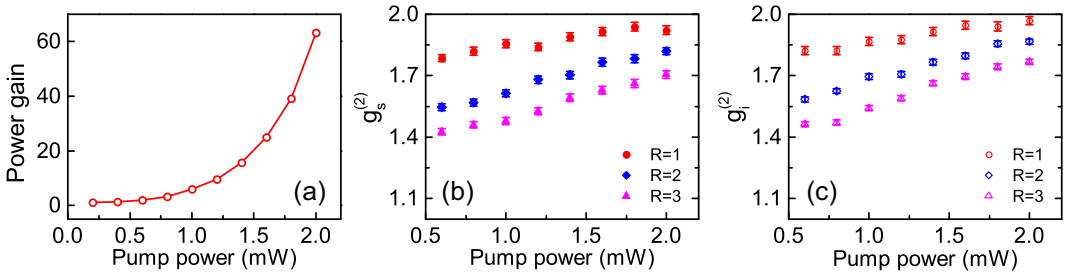

Fig. 6. (a) Power gain of amplified signal as a function of pump power when the power of the seeded reference signal is about 1 μW. The intensity correlation function in (b) signal and (c) idler bands, $g_s^{(2)}$ and $g_i^{(2)}$, versus pump power for the filter F2 with different ratio $R = \sigma_{s(i)}/\sigma_p$.

Moreover, it is worth pointing out that in DSF, the influence of higher order terms of the dispersion and the self-phase modulation term $2\gamma P_p L$ on the phase matching condition in DSF need to be considered. According to the Taylor expansion of the wave vectors at the pump frequency ω_{p0}, the phase mismatching term in DSF is approximated as $\Delta k \approx 2\gamma P_p + \frac{\beta_2}{4}\Delta^2 + \frac{\beta_2}{2}\Delta(\Omega_s - \Omega_i) + \frac{\beta_3}{8}\Delta^2(\Omega_s + \Omega_i)$, where $\Delta = \omega_{s0} - \omega_{i0}$ is the central frequency difference between signal and idler fields, β_2 and β_3 are the second and third order dispersion coefficient, respectively [28]. Optimum phase matching condition requires $2\gamma P_p + \frac{\beta_2}{4}\Delta^2 = 0$. Clearly, Δk varies with the pump power. So, we need to find out whether the increasing trend of $g_s^{(2)}$ and $g_i^{(2)}$ in Fig. 6 is caused by (i) the modification of the phase matching condition or (ii) the increased gain of SFWM.

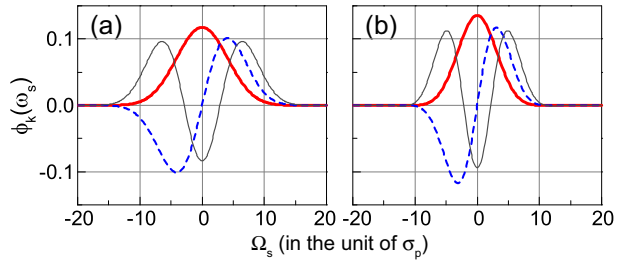

Fig. 7. Sketch map of the spectra of the first three decomposed modes in DSF, $\phi_k(\omega_s)$ ($k = 1,2,3$), for the average pump power of about (a) 0.5 mW and (b) 2 mW, respectively. The red, blue and grey curves are for the mode with index $k = 1$, $k = 2$, and $k = 3$, respectively.

We experimentally estimate the term Δk and JSF in DSF by measuring the spectrum of SFWM under different pump power. We find that under the optimized phase matching condition $2\gamma P_p + \frac{\beta_2}{4}\Delta^2 = 0$, the frequency difference $\Delta = \omega_{s0} - \omega_{i0}$ changes from 5 to 7 THz when the pump power changes from 0.5 to 2 mW. With the increase of pump power, the frequency distribution of the kth order decomposed modes, $\phi_k(\omega_s)$ and $\psi_k(\omega_i)$, become narrow, as illustrated by the first three decomposed modes $\phi_k(\omega_s)$ ($k = 1,2,3$) in Fig. 7. However, there is no observable change of $\sum_k r_k^4$ (the distribution of r_k is similar to Fig. 2(b)) when the phase matching condition is altered due to the self-phase modulation effect of pump. Consequently, when the gain of SFWM and bandwidth of filter are fixed, this spectral narrowing effect of the decomposed modes $\phi_k(\omega_s)$ ($\psi_k(\omega_i)$) results in a decreased value of $g_{s(i)}^{(2)}$ because effective mode

#253936 Received 16 Nov 2015; revised 20 Dec 2015; accepted 5 Jan 2016; published 13 Jan 2016

number of the measured fields will accordingly increase. Hence, the increasing trend of $g^{(2)}_{s(i)}$ in Fig. 6 is caused by the increased gain of SFWM, which is in agreement with our theoretical analysis.

4. Summary

In summary, we have studied temporal/spectral mode property of twin beams generated by the pulse-pumped spontaneous four wave mixing in optical fiber with the measurement of the normalized intensity correlation function of individual signal and idler beams. Our results show that the temporal property depends not only on the phase matching condition and the bandwidth of filters in signal and idler fields, but also on the gain of SFWM. Under a given phase matching condition, which determines the frequency correlation between the signal and idler twin beams in low gain regime, the normalized intensity correlation function of individual signal/idler beam increases with the gain of SFWM, indicating that the temporal/spectral behavior at high gain is dominated by the fundamental modes of the twin beams. With the gain in our experiment, we achieved near single temporal mode operation as witnessed by the measured value of $g^{(2)}_i = 1.97 \pm 0.02$. Our investigation is useful for improving the broadband noise reduction of pulsed multimode quantum light and for characterizing the pulsed quantum state [5, 15, 16, 25, 35]. Moreover, our investigation illustrates that for the application of characterizing the spectral properties of photon pairs by using intensity correlation function [32, 33], it is of great importance to ensure the operation is in the low gain regime.

Acknowledgment

This work was supported in part by the State Key Development Program for Basic Research of China (No. 2014CB340103), the National NSF of China (No. 11527808, No. 11504262), the Specialized Research Fund for the Doctoral Program of Higher Education of China (No. 20120032110055), The Natural Science Foundation of Tianjin (No. 14JCQNJC02300), PCSIRT and 111 Project B07014.

#253936 Received 16 Nov 2015; revised 20 Dec 2015; accepted 5 Jan 2016; published 13 Jan 2016